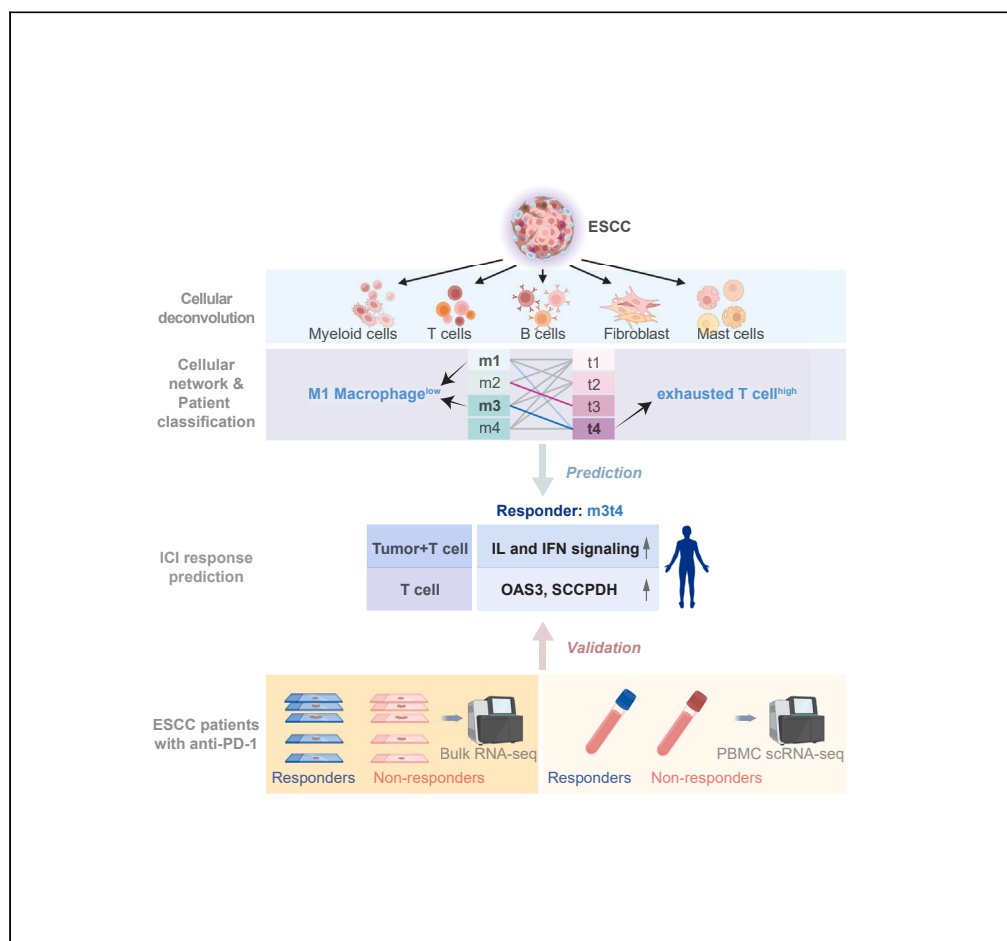# iScience

Article

Tumor niche network-defined subtypes predict immunotherapy response of esophageal squamous cell cancer

Kyung-Pil Ko,
Shengzhe Zhang,
Yuanjian Huang, ...,
Haiyang Zhang,
Zhihua Liu, Jae-Il
Park

jaeil@mdanderson.org

Highlights

Immunotherapy-sensitive
ESCC patients prediction
by scRNA-seq-based TME
profiling

Integrative analyses of T
cells and myeloid cells
predict immunotherapy
response

IL and IFN signaling
pathways in T cells
characterize the
immunotherapy
responders

Article

Tumor niche network-defined subtypes predict immunotherapy response of esophageal squamous cell cancer

Kyung-Pil Ko,[1] Shengzhe Zhang,[1] Yuanjian Huang,[1] Bongjun Kim,[1] Gengyi Zou,[1] Sohee Jun,[1] Jie Zhang,[1] Yahui Zhao,[2] Cecilia Martin,[3] Karen J. Dunbar,[3] Gizem Efe,[3] Anil K. Rustgi,[3] Hiroshi Nakagawa,[3] Haiyang Zhang,[4] Zhihua Liu,[2] and Jae-Il Park[1,5,6,7,*]

SUMMARY

Despite the promising outcomes of immune checkpoint inhibitors (ICIs), resistance to ICI presents a new challenge. Therefore, selecting patients for specific ICI applications is crucial for maximizing therapeutic efficacy. Herein, we curated 69 human esophageal squamous cell cancer (ESCC) patients' tumor microenvironment (TME) single-cell transcriptomic datasets to subtype ESCC. Integrative analyses of the cellular network and transcriptional signatures of T cells and myeloid cells define distinct ESCC subtypes characterized by T cell exhaustion, and interleukin (IL) and interferon (IFN) signaling. Furthermore, this approach classifies ESCC patients into ICI responders and non-responders, as validated by whole tumor transcriptomes and liquid biopsy-based single-cell transcriptomes of anti-PD-1 ICI responders and non-responders. Our study stratifies ESCC patients based on TME transcriptional network, providing novel insights into tumor niche remodeling and potentially predicting ICI responses in ESCC patients.

INTRODUCTION

Esophageal cancer is the seventh most prevalent cancer, and ESCC accounts for more than 80% of esophageal cancer cases worldwide.[1,2] The leading cause of death of ESCC is the sixth highest of all types of cancer as the 5-year survival rate is as low as 10–25%.[3] Despite its high incidence, the treatment option for ESCC is limited compared to the other major types of cancer. Among the multidisciplinary treatments, including surgery, neoadjuvant therapy, and chemoradiotherapy, therapeutic option for ESCC largely relies on cytotoxic reagent-based chemotherapy. However, the outcome is unfavorable.[4,5]

To overcome the limited efficacy of ESCC treatment, immunotherapy using ICIs has recently been tested in clinical trials, which resulted in survival benefits for advanced or metastatic ESCC patients.[6–8] However, approximately 34% and 25% of ESCC patients discontinued ICI treatment because of disease progression[8] and severe adverse effects,[9,10] respectively. In recent clinical trials, the ICI response rate of ESCC patients was only 13–28%.[9–16] Although the clinical trials using ICIs are mainly applied to patients diagnosed with advanced or metastatic ESCC, pathologic criteria used for selecting patients for ICIs remain to be clarified.[5] Although modern pathological criteria, such as PD-L1 expression in tumor cells, are utilized, it is increasingly recognized that host-intrinsic factors, specifically the immune system, play a pivotal role in determining the response to ICIs.[17] Therefore, the stratification of patients based on their individual immune cell characteristics becomes crucial in enhancing the effectiveness of immunotherapy.

TME, a cellular niche surrounding tumor cells, includes immune cells, fibroblasts, and endothelial cells.[18] Accumulating evidence suggests that TME plays a crucial role in tumor progression, metastasis, therapy resistance, and immune evasion.[19] Along with the advent of single-cell transcriptomics, the oncogenic functions of TME in ESCC tumorigenesis have been recently unraveled. Several studies characterized ESCC TME as creating an immunosuppressive environment.[20–23] In addition to the conventional cancer classification, which mainly relies on the pathologic stages,[24] transcriptome-based cancer classification has recently been introduced in several cancer types.[25,26] Simultaneously, profiling cancer immune systems or cancer-associated fibroblasts (CAFs) identified tumorigenic roles of tumor-infiltrated immunocytes

[1]Department of Experimental Radiation Oncology, Division of Radiation Oncology, The University of Texas MD Anderson Cancer Center, Houston, TX 77030, USA
[2]State Key Laboratory of Molecular Oncology, National Cancer Center, National Clinical Research Center for Cancer, Cancer Hospital, Chinese Academy of Medical Sciences and Peking Union Medical College, Beijing 100021, China
[3]Division of Digestive and Liver Diseases, Department of Medicine, Herbert Irving Comprehensive Cancer Center, Columbia University Irving Medical Center, New York, NY 10032, USA
[4]Key Laboratory of Cancer Prevention and Therapy, Tianjin, Tianjin's Clinical Research Center for Cancer, National Clinical Research Center for Cancer, Tianjin Medical University Cancer Institute and Hospital, Tianjin, China
[5]The University of Texas MD Anderson Cancer Center UTHealth Houston Graduate School of Biomedical Sciences, Houston, TX 77030, USA
[6]Program in Genetics and Epigenetics, The University of Texas MD Anderson Cancer Center, Houston, TX 77030, USA
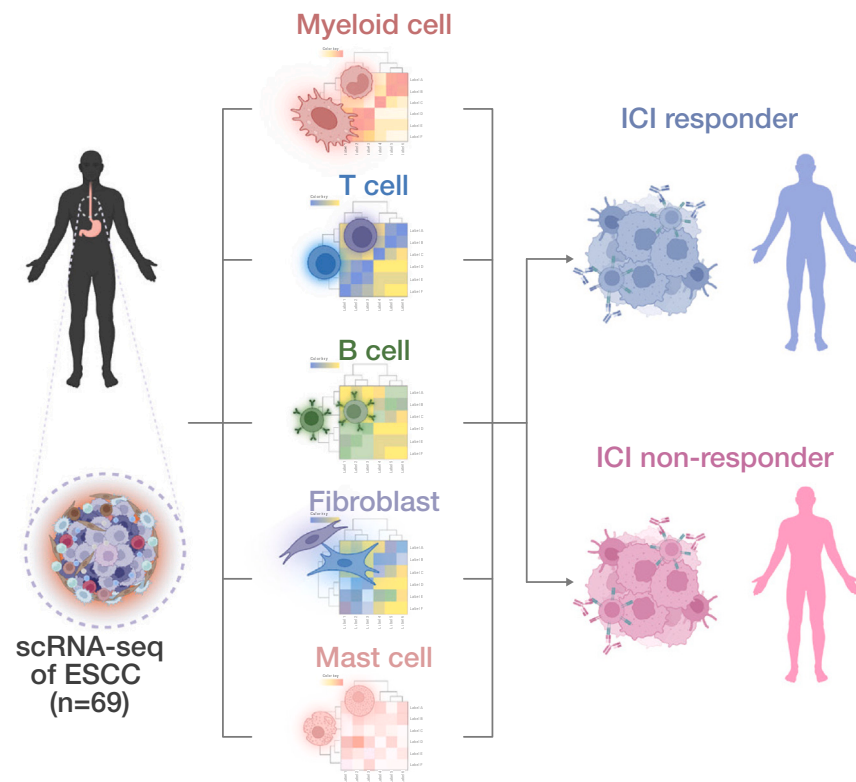[7]Lead contact
*Correspondence: jaeil@mdanderson.org
https://doi.org/10.1016/j.isci.2024.109795

Figure 1. Schematic workflow for transcriptomic analysis of TME from ESCC patients

and CAFs, which also gained attention.[27,28] Nonetheless, comprehensive dissection and characterization of ESCC TME still needed to be achieved. Moreover, how distinct TMEs define immune evasion and ICI response of ESCC remains to be determined.

Herein, we analyzed 69 single-cell transcriptomic datasets of ESCC patients' primary tumor samples and characterized whole TME. Intriguingly, comprehensive analyses of TME identified the distinct networks mainly between T cells and myeloid cells, which define specific subtypes and immunosuppression of ESCC.

RESULTS

TME transcriptome-based classification of ESCC patients

For the TME-based ESCC characterization, we analyzed single-cell RNA-sequencing (scRNA-seq) datasets of ESCC patient tumors from 69 patients (Figure 1). All datasets were integrated using the Harmony algorithm[29] and processed to analyze only non-epithelial cells (*EPCAM* negative) comprising ESCC TME (Figures 2A and 2B). Unsupervised transcriptomic clustering revealed several immune cell types, fibroblasts, and mast cells (Figures 2C and S1A). Since T cells play a pivotal role in eliciting an immunogenic response to tumor cells, we first analyzed T cell clusters.[30,31] T cell clusters were isolated and processed into the subgroups (Figure 2D). The unsupervised clustering using principal component analysis (PCA) and Pearson's correlation categorized T cells of 69 datasets into four groups (t1, t2, t3, and t4) (Figure 2E). On the Uniform Manifold Approximation and Projection (UMAP), T cells of t1 and t2 groups were closely located together. In contrast, the t4 group was slightly distinct from the t1 and t2 groups (Figure 2F). Notably, the t3 group was the most distantly located on the UMAP, suggesting the relatively low similarity of t3 transcriptome to those of t1, t2, and t4 groups (Figure 2F). To define subsets of T cells, we annotated T cells based on the known marker genes expression (Figures 2G, S1B, and S1C). In a detailed cell subset analysis, T cells of the t3 group showed the most abundance in CD8 T cells, while the other subsets (t1, t2, and t4) rarely exhibited CD8 T cells (Figure 2G). Besides, T cells of the t4 group showed the highest proportion of exhausted T cells (T_{ex}) compared to the other three groups (Figure 2G). Since t3 is the distinct subgroup, we further analyzed the T cells of the t3 group. After excluding the CD4 T cell cluster, we found that t3 group T cells can be classified into several memory T cells based on the marker genes of subsets (Figures S1D and S1E).[32,33] Interestingly, early memory T cells (Tem-early) and peripheral memory T cells (Tpm) were observed to be the most abundant cells in the t3 group compared to the other subsets (Figure S1F). These results indicate that the t4 group of patients is mainly characterized by T cell exhaustion, whereas the t3 group is enriched with active CD8 T cells.

In addition, we comparatively analyzed myeloid cell clusters of 69 datasets (Figure 2H). Similar to T cell analysis, Myeloid cells transcriptomes were classified into four groups (m1, m2, m3, and m4) based on the principal component analysis and Pearson's correlation (Figure 2I). Myeloid cells of m1, m3, and m4 showed close location on the UMAP. In contrast, m2 cells were distinguishable from m1, m3, and m4.
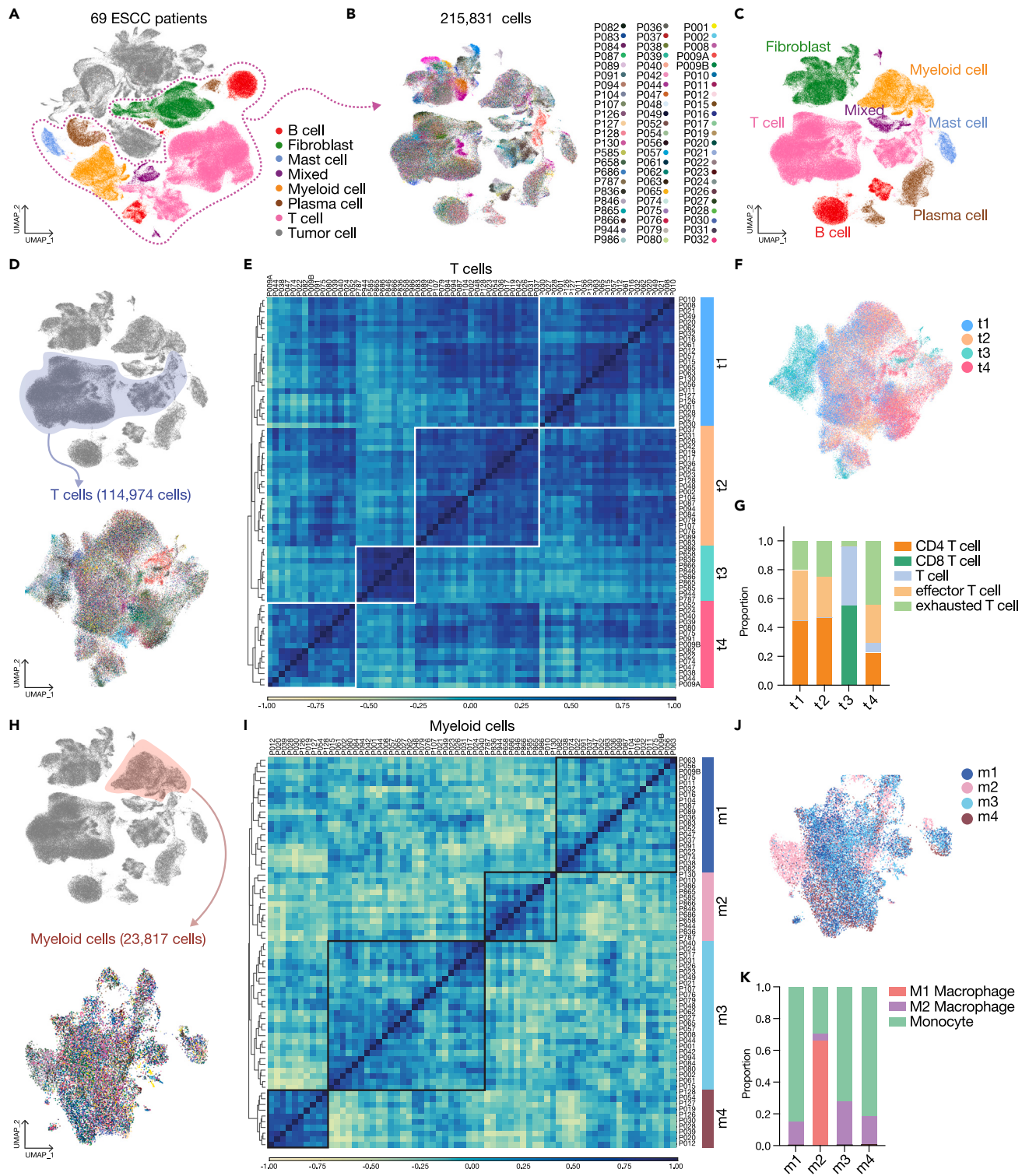
Figure 2. Immune cells analysis and classification

(A) Uniform Manifold Approximation and Projection (UMAP) display of whole cells from 69 patients. Single-cell RNA-sequencing (scRNA-seq) results of the cells of TME were integrated and projected.

(B and C) Non-tumor cells were isolated, and UMAP was redrawn with individual patient information (B) and five major cell types (C).

(D) UMAP display of T cells subgroup with unique patients ID. T cells were isolated from immune cells and clustered again.

Figure 2. Continued

(E) T cells were classified into four sub-groups by principal component analysis (PCA) and Pearson correlation. PCA result was clustered by the dendrogram, and Pearson correlation was displayed by color spectrum.

(F) T cells were displayed in UMAP based on the sub-groups defined from PCA and Pearson correlation.

(G) Each sub-groups of T cells were shown with subsets using stacked bar plots.

(H) Myeloid cells of each patient were displayed with UMAP. Myeloid cells were isolated from immune cells and clustered independently.

(I) Myeloid cells were categorized into four sub-groups by PCA and Pearson correlation. PCA results were displayed with a dendrogram, and Pearson correlation was shown by color spectrum.

(J) Myeloid cells were displayed with sub-groups identified from PCA and Pearson correlation.

(K) Each myeloid cell sub-group was displayed with subsets of myeloid cells.

(Figure 2J). Interestingly, based on the clustering with marker genes, m2-grouped myeloid cells were enriched with M1 macrophages, whereas possessing the least proportion of M2 macrophages compared to those of the other three groups (m1, m3, and m4) (Figures 2K and S1G). These results imply that the ESCC patients in the m2 group might have tumor-unfavorable myeloid cells compared to the other groups.

Single-cell transcriptomes of myeloid and T cells define immunosuppressive ESCC subtypes

We next evaluated which group of T cells exhibits the most immunosuppressive characteristics by assessing the expression of T_{ex} markers. The t4 group expressed the highest level of *LAG3, PDCD1,* and *HAVCR2,* whereas the t3 group barely expressed the T_{ex} cell markers (Figures 3A and S2A). To test if the T cell category correlates with myeloid cell classification, we compared the number of patients of each T cell group in the myeloid cell group. Interestingly, patients of t3, the least T_{ex}-characterized group, mostly belonged to the m2 categories. In contrast, t4-grouped patients, the enriched T_{ex}-characterized group, were mainly distributed to m1-or m3-grouped patients (Figures 3B and 3C). Accordingly, we combined the categories of T cells and myeloid cells to make 12 sub-groups (MT groups) of patients (Figure 3D). We observed that the m2t3 group was separated from other cell clusters in the T cell UMAP. The m1t4 or m3t4 groups were slightly distinct from the major population of T cells in the UMAP (Figure 3E). We also identified that T cells of m1t4 and m3t4 groups exhibited the highest expression of T_{ex} cell markers. Conversely, T cells of the m2t3 group showed the lowest expression of those markers (Figures 3F, S2B, and S2C). Based on these findings, we analyzed m1t4 and m3t4 groups of patients since these groups showed the highest expression of T_{ex} markers in T cells. In the GSEA analyses comparing m1t4 or m3t4 with the m2t3 group of T cells, both m1t4 and m3t4 groups displayed enrichment of 'Negative regulation of lymphocyte activation', 'IFN α/β signaling', and 'Signaling by ILs' (Figures 3G and S2D), implying that T cells of m1t4 and m3t4 groups are enriched with type I IFN and IL signaling pathways. Additionally, from the GSEA of tumor epithelial cell and myeloid cells, epithelial cells of m1t4 and m3t4 groups were observed to show enriched 'IFN α/β signaling', consistent with the result from T cell (Figures S2E and S2F). Furthermore, we next performed cell-to-cell interaction analysis in m1t4, m2t3, and m3t4 groups using the 'CellChat' package that infers cellular interactome based on ligand-receptor expressions.[34] Interleukins and IFN-related cell-to-cell communications were enriched in m1t4 and m3t4 between monocyte, T cells, and tumor cells, while m2t3 group did not show significant communication (Figures 3H and 3I). These results suggest that m1t4 and m3t4 groups are characterized by T cell exhaustion and enriched IFN and IL signaling pathways activation compared to the other groups.

Subgroups analyses defined by B cells, fibroblasts, and mast cells

For a comprehensive analysis of ESCC TME, we further examined B cells, fibroblasts, and mast cells. We analyzed B cell clusters of 69 ESCC datasets based on their transcriptomic similarity (Figure S3A). The correlation matrix of B cells identified two subgroups (b1 and b2) of patients (Figures S3B and S3C). Interestingly, more than half of b2 sub-grouped-patients (62.5% [10/16]) overlapped with those of the t3 subgroup (Figures S3D and S3E). Meanwhile, the t4 subgroup characterized by abundant T_{ex} cells was mainly assigned to b1 subgroups (85.7% [12/14]) (Figures S3D and S3E). We constructed combined BT groups connecting B cell groups and T cell groups and examined their T cells by evaluating the expression of exhausted T cell markers (Figures S3F and S3G). The b1t4 subgroup expressed the highest level of T_{ex} cell markers compared to the others. On the other hand, the b2t3 group showed the most negligible expression of T_{ex} cell markers (Figure S3H). Based on this finding, we compared the T cells of the b1t4 and b2t3 groups (Figure S3H). We comparatively analyzed b1t4-and b2t3-categorized T cells using GSEA. 76 results overlapped in the b1t4-positively significant and the b2t3-negatively significant signaling pathways (Figure S3I). Interestingly, among those overlapped signaling, we found that ILs and IFN signaling pathways were positively enriched in b1t4-grouped T cells (Figure S3J). Overall, b1t4 group showed similar phenotypes of m1t4 and m3t4. However, B cell-based classification did not efficiently categorize the patients since most of patients (76.5%, [52/68]) were assigned to the b1 group (Figure S3K).

Fibroblasts from tumor datasets were isolated using fibroblast marker genes and analyzed independently to explore their correlation with T cells (Figure S4A). Based on transcriptomic comparisons (Figures S3B and S3C), patients were categorized into two groups, f1 and f2, and connected to the T cell group information (Figure S3D). Interestingly, a significant portion of patients in the t4 group were assigned to the f2 group, while the f1 group predominantly consisted of the t3 group (Figures S3D and S3E). However, due to the high proportion of the f2 group, a considerable number of patients from the t1 and t2 groups were also included in the f2 group (Figures S4E and S4F). When examining the FT group, which combined fibroblast groups with T cell groups, we observed that exhausted T cell markers were predominantly expressed in the f2t4 group, while the f1t3 group exhibited minimal expression of these markers (Figures S4G and S4H). However, compared to the MT
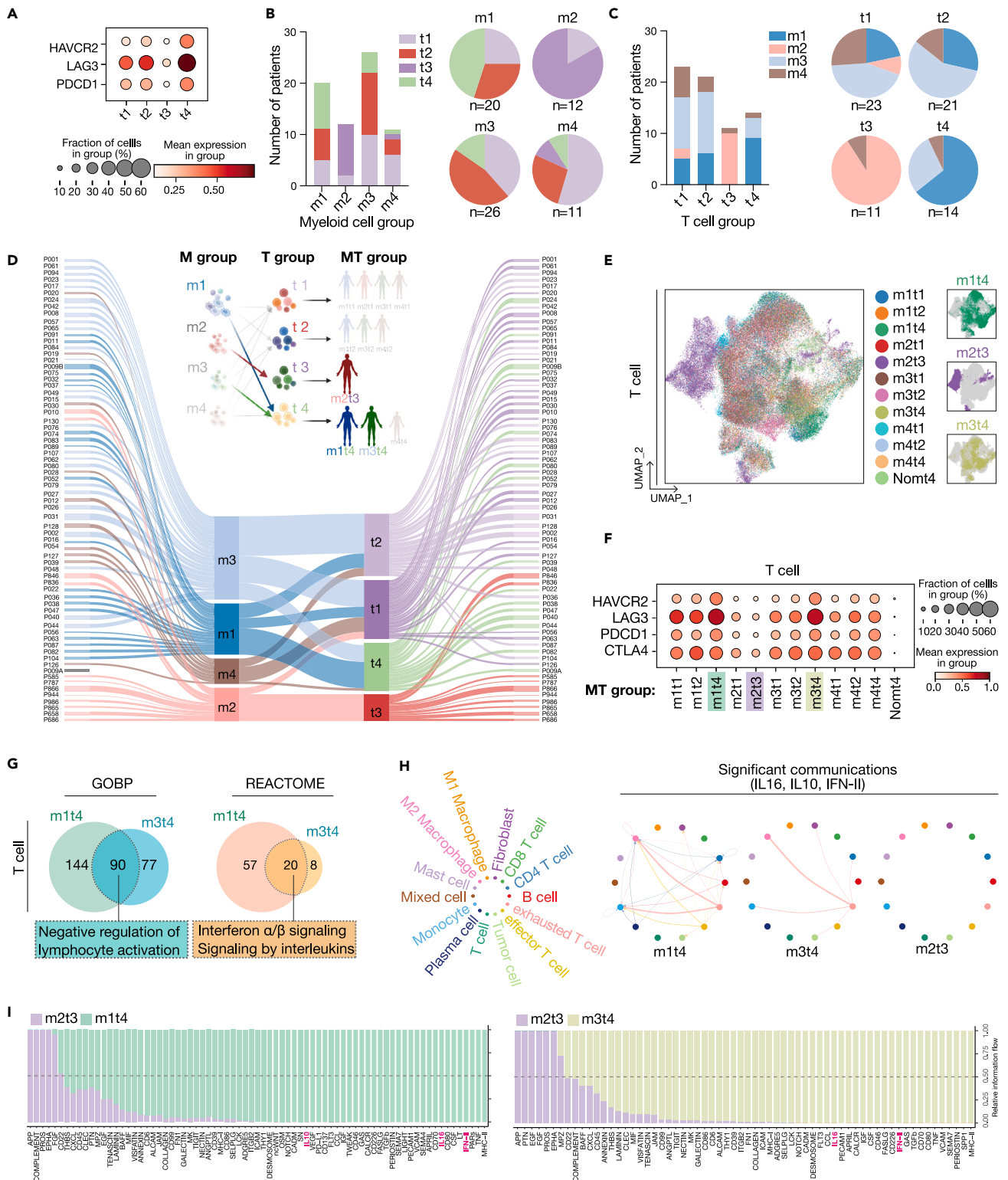
Figure 3. Comparative analysis of patients by myeloid and T cell classifications

(A) T$_{ex}$ cell markers expression in each T cell sub-group.

(B) The number and proportion of patients of T cell-sub-groups were displayed in each patient's sub-groups categorized by myeloid cells.

Figure 3. *Continued*

(C) The number of sub-grouped patients by myeloid cell was displayed in each patient's sub-groups categorized by T cells. The proportion of myeloid-cell-based classified patients in each sub-group of T cells was shown with pie plots.

(D) Individual patients were subjected to each sub-group of myeloid and T cells by Sankey plot. P009A patient was not included in the myeloid cell-based sub-group due to the lack of myeloid cells in the dataset. Each patient was classified into 12 groups (MT groups) by sub-groups of myeloid cells and T cells and categories.

(E) T cells of each patient from 12 groups were displayed with UMAP.

(F) T_{ex} cell markers expression in T cells in the MyT groups of patients.

(G) GSEA analysis was performed in T cells of MT groups of patients. The results of GSEA from the m1t4 and m3t4 groups of patients were compared. GOBP and REACTOME databases were used, and the significant signaling pathways with positive values of NES were compared. Overlapped signaling pathways were displayed with a Venn diagram.

(H and I) Cell-to-cell interactions were inferred using the CellChat analysis package. Tumor cells and TME cells of m1t4, m2t3, and m3t4 grouped patients were analyzed, and significant IL1, IL16, IL10, and IFN-II signaling pathways-related interactions were visualized with circle plot (H), m1t4 and m3t4 grouped patients were compared with m2t3 grouped patients to identify specific signaling pathways (I).

classification, the fibroblast-based patient grouping did not effectively classify patients when combined with T cell groups, primarily due to a bias toward the f2 group (Figure S4K).

We also analyzed the mast cells for classification (Figure S5A). 3,864 cells were segregated from TME datasets and processed for calculating transcriptomic similarity (Figure S5B). However, the difference in transcriptomes represented by Pearson's correlation was insufficient to make subgroups. Collectively, B cell- and Mast cell-based classification did not properly segregate patient groups compared to T or MT classification.

Pathological relevance of TME transcriptomes to anti-PD-1 immunotherapy response

The findings obtained through myeloid and T cell classification led us to hypothesize that m1t4 and m3t4 groups of patients may exhibit enhanced responsiveness for ICI treatment. To test this hypothesis, we conducted analyses using two independent datasets: scRNA-seq dataset from peripheral blood mononuclear cells (PBMC) and bulk RNA-seq dataset from tumor-embedded slide. First, we tested if our classified immune cells match the immune cells of responding patients treated with anti-PD-1 immunotherapy. The reference patients were collected and grouped into responders (PBMC-R, $n = 3$) and non-responders (PBMC-NR, $n = 3$) by their sensitivity to the anti-PD-1 antibody treatment (Figure 4A). Cell types, including T cell, B cell, monocyte, neutrophil, and platelet, were annotated after integrating PBMC datasets (Figures 4B–4D). As expected, T_{ex} markers (TIGIT, HAVCR2, LAG3, and CTLA4) were observed to be more highly expressed in responders than in non-responders, indicating that patients who are susceptible to ICI exhibit the higher T_{ex} signature not only in tumor niche, but also in their PBMCs compared to the non-responders (Figures 4E, S6A, and S6B). Next, to identify the signaling pathway signatures of T cells, we performed GSEA in PBMC-R and PBMC-NR and compared the results with those from m1t4, m3t4, and b1t4 groups. Interestingly, we found that 'PD-1 signaling', 'Interferon signaling', and 'Signaling by ILs' were commonly enriched in PBMC-R as well as m1t4, m3t4, and b1t4 groups (Figures 4F–4H, S6C, and S6D). Moreover, T cell scoring analysis using PD-1, IFN, and ILs signaling pathways-related genes showed higher scores in PBMC-R, m1t4, m3t4, and b1t4 groups compared to PBMC-NR, m2t3, and b2t3 groups, respectively (Figure S6E). These results echo the importance of IFN and IL signaling pathways in immunotherapy-sensitive patients, as we found from m1t4-and m3t4-grouped patients (Figures 3G–3I). To increase the credibility of validation, we also analyzed the bulk RNA-seq datasets created from ICI responders (Tumor-R, $n = 7$) and non-responders (Tumor-NR, $n = 10$) (Figure 4I).[35] Since bulk RNA-seq results cannot provide cell type-specific information, we integrated 17 patient datasets and analyzed the global transcriptomes or signaling pathway signatures (Figure S6F). Intriguingly, in the Enrichr analysis and GSEA, we found that Tumor-R also showed enriched signaling pathways related to IFN and ILs, which is consistent with m1t4-and m3t4-grouped patients (Figures 4J and S6G). To avoid over-emphasis by a few signaling pathways, we conducted a direct transcriptomic comparison using the Scissor package, a tool to find bulk RNA-seq-based transcriptomic signature-associated cells from scRNA-seq.[36] First, we binarized gene expression pattern based on the Tumor-R and Tumor-NR groups and compared the signatures in each cell of the m1t4, m2t3, and m3t4 groups. Strikingly, we found that Tumor-R-similar cells (Tumor-R$^+$) are more accumulated in the m1t4 and m3t4 datasets, especially in the myeloid cell and T cell clusters. On the other hand, m2t3 dataset showed much fewer Tumor-R$^+$ cells throughout the cell clusters compared to the others (Figures 4K and 4L). The discovery that the transcriptomes of immune checkpoint inhibitor (ICI) responders exhibit greater similarity to T cells and myeloid cells rather than tumor cells was highly unexpected. However, this finding highlights the crucial significance of host-intrinsic factors in identifying molecular signatures associated with ICI efficacy. In this transcriptomic comparison, m3t4 showed a greater number of Tumor-R$^+$ cells compared to m1t4 and m2t3 although it has a smaller number of total cells, which led us to further identify the most probable as a predicted responder (Figures 4M and 4N).

Identification of the most responders-like patient group

Since transcriptomic comparison can identify the most similar group based on a large number of gene expression information, we employed this method to compare our MT-grouped patients with two different reference datasets. To this end, we prepared 69 ESCC TME datasets ($n = 69$) with or without tumor epithelial cells to compare with bulk RNA-seq dataset and immune cell scRNA-seq dataset, respectively (Figure 5A). First, to analyze transcriptomes of ESCC scRNA-seq (MT groups) with bulk RNA-seq (Tumor-R and -NR), we made a single matrix from scRNA-seq dataset including tumor cells and TME cells to make a pseudo-bulk RNA-seq dataset. This pseudo-bulk RNA-seq dataset was
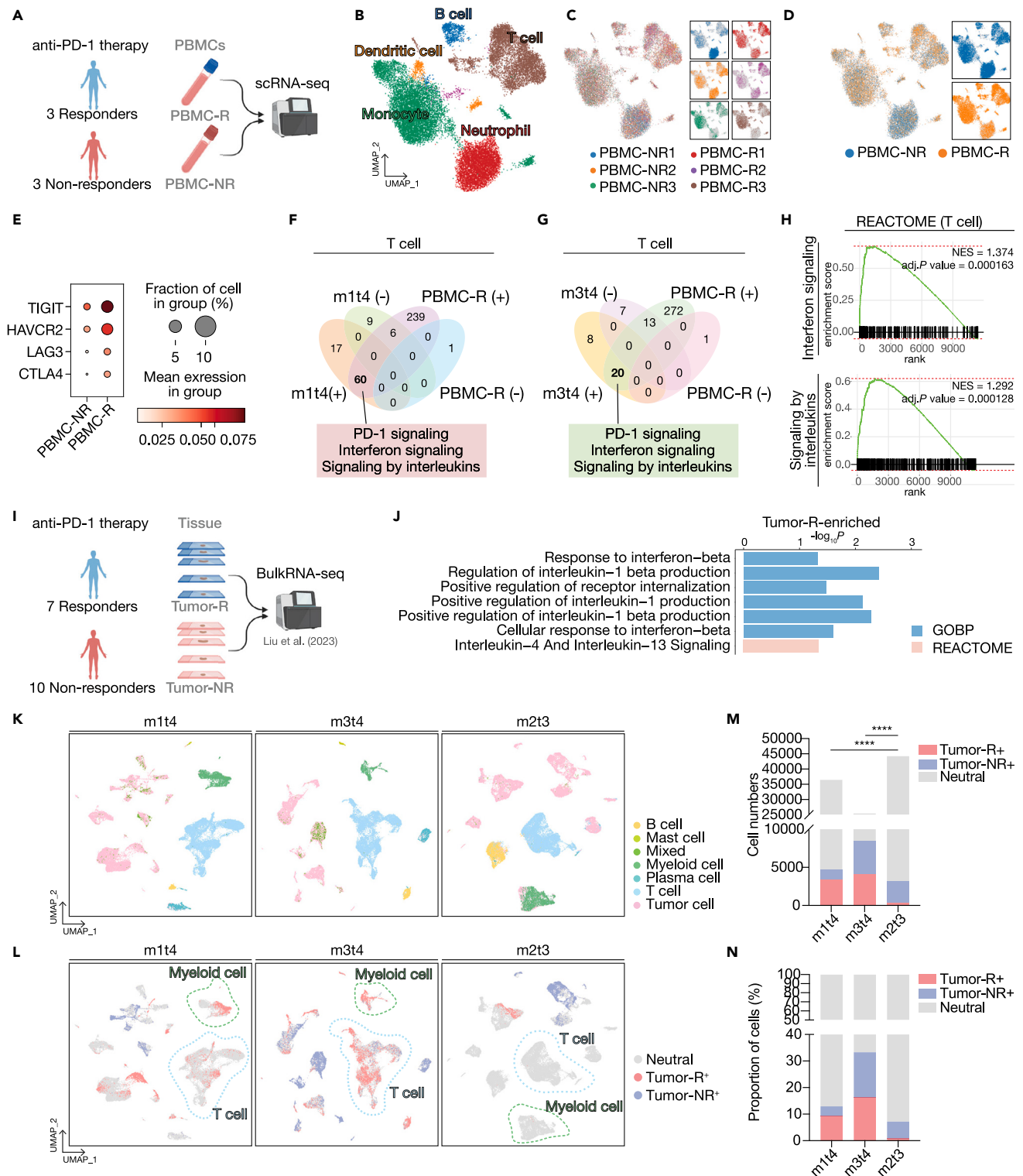
Figure 4. Validation of predicted responders by anti-PD-1 immunotherapy-treated patients

(A–D) Peripheral blood immune cells transcriptomes of three responders (PBMC-R) and three non-responders (PBMC-NR) (to anti-PD-1 ICI) were integrated and presented with UMAP by cell types (A, B), patients (C), and response groups (PBMC-R vs. PBMC-NR) (D).

(E) T_{ex} marker genes expression was compared by the anti-PD-1 response (R vs. NR).

Figure 4. Continued

(F–H) GSEA analysis performed in T cells of PBMC-R vs. PBMC-NR groups using the REACTOME database. Significant results with positive NES and negative NES were compared with the results of m1t4 (F) and m3t4 (G). Enrichment plots of PD-1 signaling and Interferon signaling were displayed (H).

(I) Bulk RNA-seq datasets of responders (Tumor-R) and non-responders (Tumor-NR) were collected and analyzed.

(J) Pathway signatures of Tumor-R were analyzed using enrichr through comparison with the Tumor-NR group.

(K–N) Transcriptomes of Tumor-R and Tumor-NR were compared with single-cell transcriptomes of three MyT groups using the Scissor package. Each MyT group dataset was prepared by integrating tumor cells and TME cells (K). Cells of Tumor-R phenotypes were displayed in red, and Tumor-NR phenotypes were in blue. Cells not assigned to Tumor-R or Tumor-NR were annotated as neutral cells (L). Results of the Scissor analysis in three groups were compared using barplots with absolute cell numbers (M) and proportion (N). ****p values < 0.0001, as determined by Fisher's exact test.

eventually integrated with the bulk RNA-seq datasets (Tumor-R and -NR) and analyzed using the PCA method (Figure 5B). The most proximal dataset to Tumor-R was m3t4 compared to the other groups (Figure 5C). Simultaneously, TME cells of ESCC scRNA-seq datasets were integrated and compared with immune cell transcriptomes of PBMC-R and -NR to perform PCA (Figure 5D). The m3t4 groups was also hierarchically closer to PBMC-R compared to the other groups (Figure 5E). Consistent with the findings, GSEA analysis of epithelial cells of MT group and Tumor-R group identified eight overlapped signaling pathways between Tumor-R only with m3t4, while m1t4 group did not show any shared signaling pathways (Figure 5F). These findings suggest that m3t4 has the most similar transcriptomes to the ICI-responders. Therefore, we sought to find m3t4 and responders exclusive features which are not overlapped with m1t4. From the GSEA analysis of T cell cluster, we found several overlapped significant signaling pathways specific to m3t4 and Responders (Tumor-R and PBMC-R), such as 'IL-6 production,' 'Regulation of ion transport,' 'IFN-γ production,' 'Response to FGF,' 'Viral genome replication,' 'Platelet activation signaling and aggregation,' and 'Semaphorin interactions' (Figures 5G and 5H). Among them, FGF and IFN-γ scores were consistently higher in m3t4 and responders (Figure 5I). In contrast, HSF1-related signaling pathways were exclusively enriched in m1t4 (Figures 5H and 5I). For gene expression level, OAS and SCCPDH expressions were significantly higher in m3t4 and PBMC-R T cells (Figures 5J and S7A–S7D). These results suggest that the signaling pathway signatures and molecular signatures of m3t4 T cells are conserved in the T cells of responders' PBMC samples.

DISCUSSION

To enhance the efficacy and minimize the adverse effects of cancer therapies, it is crucial to subtype and characterize patients, selecting those who will benefit most from specific treatments. In this study, we curated a significant number of single-cell transcriptome datasets from ESCC primary tumors, establishing precise patient categories based on TME transcriptomes beyond conventional and molecular pathology. We discovered that combining the transcriptional signatures of myeloid cells with T cells (MT) can effectively stratify ESCC patients, possibly predicting the outcomes of immunotherapy treatment. Specifically, patients classified as m1t4 and m3t4 displayed the T_{ex} cells phenotype in their T cells, suggesting a promising response to ICI. Conversely, patients categorized as m2t3 were unlikely to respond to ICI, as their T cells rarely exhibited T cell exhaustion. Based on these findings, m1t4 and m3t4 groups were expected to exhibit an improved response to ICI treatment. This hypothesis was primarily supported by the growing evidence of the favorable outcomes observed in patients with elevated expression levels of immune checkpoint molecules following ICI therapy.[37,38] Furthermore, our analysis of reference immune cell datasets, specifically PBMC-R and PBMC-NR, indeed displayed higher expression of exhausted T cell markers.

The inclusion of myeloid cell characteristics alongside T cell classification in our study stems from the recognition that the process of T cell exhaustion does not solely rely on T cells' intrinsic pathways. Previous studies have indicated that T cell exhaustion is influenced by multiple factors, including cytokines released by cells within the TME.[39,40] In this regard, we identified several signaling signatures related to IFN and IL, which establish an interaction network between myeloid cells (monocyte and M2 macrophage) and T cells (CD4 T cell and exhausted T cell) in the m1t4 and m3t4 groups (Figure 3). Notably, cytokines such as type I IFNs, IL-6, IL-10, and IL-27 were reported to induce T cell exhaustion.[39,41] Although a majority of studies focused on the roles of the anti-tumor effect of IFN α/β, recent studies revealed that type I IFN protects cancer cells from T cell-mediated cytotoxicity.[42,43] Furthermore, persistent IFN signaling activation induces resistance to ICI therapy.[42,44] Since IFN and IL signaling pathways were consistently enriched in ICI responders (Figure 4), these pathway signatures can serve as molecular signatures for predicting the efficacy of ICI application.

In our study, despite the shared signaling pathways of ICI responders, m1t4 and m3t4 groups, we conducted a more detailed analysis to identify the most probable group to exhibit sensitivity to ICI treatment. To this end, we performed a comprehensive whole transcriptomic comparison, and disclosed m3t4 as the best candidate for the ICI treatment since this group showed the closest proximity to ICI responders. Based on these findings, we identified m3t4 T cell-specific signaling signatures (IFN-γ and FGF) followed by molecular signatures (OAS3 and SCCPDH). Given that these molecular signatures were consistently enriched in the ICI responders' T cells from PBMC, we expect that these molecules hold potential as liquid biopsy markers for the selection of patients eligible for ICI treatment (Figure 5). Although current immunotherapy primarily focuses on T_{ex} cell markers, our MT classification is expected to provide a better prediction for ICI response than grouping patients solely based on T_{ex} markers.

From a treatment perspective, while the m3t4 group is expected to respond to ICI treatment, the m1t4 group may require additional approaches to enhance ICI efficacy. One potential option for treating m1t4-like patients is the inhibition of heat shock factor 1 (HSF1)-mediated heat shock protein (HSP) signaling, which was found to be exclusively significant in m1t4 T cells (Figure 5H). Studies conducted on inflammatory diseases have demonstrated that activation of the HSP signaling pathway can induce the differentiation of regulatory T cells (T_{reg}).[45–47] Given that T_{reg} cells exert immunosuppressive effects by interacting with dendritic cells and CD8 T cells,[48,49] it is plausible that the m1t4
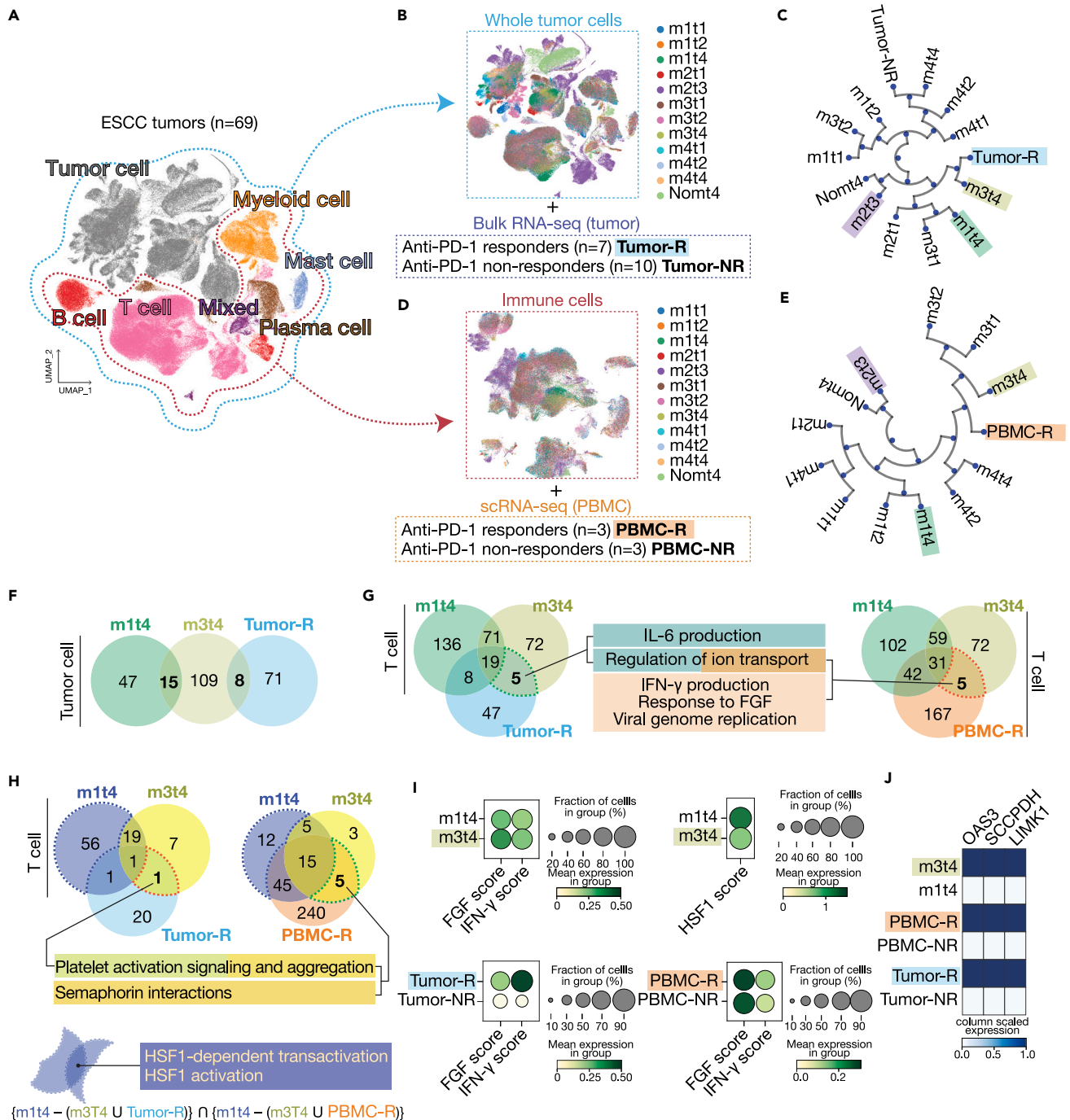
Figure 5. Specific similarity of m3t4 group with ICI-responders

(A) scRNA-seq datasets, including tumor cells and TME cells of 69 ESCC patients, were prepared to compare with ICI responders and non-responders.

(B) 69 patients' datasets, including tumor cells and immune cells, were converted to a single matrix categorized by MT groups to integrate with transcriptomes with bulk RNA-seq datasets (Tumor-R and -NR).

(C) Transcriptomes of MT groups and Tumor-R and -NR groups were compared using PCA analysis and displayed with circular dendrogram.

(D) single-cell transcriptomes of PBMC-R and PBMC-NR were integrated with 69 ESCC patients' TME transcriptomes.

(E) Correlation of MT patient groups with the PBMC-R group was analyzed using PCA and shown by the dendrogram.

(F) GSEA results of tumor cells of m1t4 and m3t4 were compared with that of the Tumor-R group using Venn diagrams.

(G) T cells of m1t4 and m3t4 were analyzed with GSEA (database: GOBP) and compared with GSEA results of Tumor-R and T cells of PBMC-R groups. Overlapped pathways of m3t4-Tumor-R and m3t4-PBMC-R were also highlighted.

Figure 5. Continued

(H) GSEA (database: REACTOME) results from T cells of m1t4 and m3t4, Tumor-R, and T cells of PBMC-R. m1t4 exclusive pathways were highlighted. Overlapped pathways of m3t4-Tumor-R and m3t4-PBMC-R were also highlighted.

(I) Pathway scores of FGF, IFN-gamma, and HSF1 in m1t4, m3t4, Tumor-R, Tumor-NR, PBMC-R, and PBMC-NR groups were shown with dotplots.

(J) Gene expression levels of OAS3, SCCPDH, and LIMK1 in m1t4, m3t4, Tumor-R, Tumor-NR, PBMC-R, and PBMC-NR groups were shown with heatmaps.

groups exhibit an additional suppressive immune landscape beyond T_{ex} cells. Thus, a potential therapeutic strategy for m1t4-like patients could involve targeting the HSP signaling pathway in combination with ICIs. This approach holds promise for mitigating the suppressive immune landscape and enhancing the effectiveness of ICI therapy in m1t4-like patients.

In this study, our main emphasis was on investigating the host-intrinsic factors that influence the response to ICIs. To achieve this, we utilized the extensive ESCC TME transcriptomes available and validated our hypothesis by comparing them with two reference data derived from patient samples with prior immunotherapy experience. By integrating results from bulk RNA-seq of the tumors and scRNA-seq of PBMC, we were able to bridge the gap between crude information obtained from bulk RNA-seq and indirect information derived from PBMC scRNA-seq. This integration allowed us to identify the most probable candidates for ICI treatment in ESCC. Through this novel approach, our study suggests the transcriptomic and molecular host-intrinsic signatures that can predict ICI responsiveness.

In conclusion, our study provides valuable insights into subtyping and characterizing ESCC patients for optimized cancer therapy. By integrating TME single-cell transcriptome datasets, we identified a specific group, m3t4, that may exhibit sensitivity to ICI treatment. We emphasized the importance of considering intrinsic T cell pathways and cytokine-mediated interactions within the TME in predicting ICI response. Moreover, the diagnostic significance of specific molecular signatures within the m3t4 group was suggested to aid in predicting ICI efficacy. This diagnostic approach has the potential to guide personalized treatment selection and improve outcomes for patients with ESCC.

Limitations of the study

Despite our efforts to collect a substantial number of reference datasets, the availability of datasets remains limited due to the relatively short history of immunotherapy in ESCC patients. In addition, the lack of gene expression data from the TME cells and clinicopathological information posed a challenge. To enhance the accuracy of prediction, further investigation using matching datasets from patients treated with immunotherapeutic agents is necessary.

Although this study stratified the ESCC patients and identified predictive signatures for immunotherapy sensitivity, the significance of these signatures requires further demonstration. We recently revealed genetic alterations of *TP53*, *NOTCH1*, and *CDKN2A* genes (PCN) induce tumorigenesis and immune evasion through releasing cytokine, CCL2, in organoid system.[50] To substantiate our findings, this PCN organoid tumor model can be used to evaluate IFN and IL signature signaling pathways in preclinical models. Moreover, we conducted additional analyses of the tumor epithelial cell transcriptomes of 69 patients, which will allow for the testing of the m3t4 and m2t3 relevant tumor models by connecting information acquired from epithelial cells and TME cells in our further study.

STAR★METHODS

Detailed methods are provided in the online version of this paper and include the following:

- KEY RESOURCES TABLE
- RESOURCE AVAILABILITY
  - Lead contact
  - Materials availability
  - Data and code availability
- METHOD DETAILS
  - scRNA-seq data preparation
  - scRNA-seq data analysis
  - PBMCs scRNA-seq data analysis
  - Bulk RNA-seq data analysis
- QUANTIFICATION AND STATISTICAL ANALYSIS

SUPPLEMENTAL INFORMATION

Supplemental information can be found online at https://doi.org/10.1016/j.isci.2024.109795.

AUTHOR CONTRIBUTIONS

K.-P.K. and J.-I.P. conceived and designed the experiments. K.-P.K., S.Z., Y.H., B.K., G.Z., S.J., and J.Z. performed the experiments. K.-P.K., H.N., H.Z., and J.-I.P. analyzed the data. C.M., K.J.D., G.E., A.-K.R., and H.N. analyzed the ESCC data. Y.Z. and Z.L. provided the bulk RNA-seq datasets and H.Z. provided the single-cell RNA-seq datasets of PD-1-treated patients. K.-P.K. and J.-I.P. wrote the manuscript.

DECLARATION OF INTERESTS

The authors declare no competing interests.

REFERENCES

1. Sung, H., Ferlay, J., Siegel, R.L., Laversanne, M., Soerjomataram, I., Jemal, A., and Bray, F. (2021). Global Cancer Statistics 2020: GLOBOCAN Estimates of Incidence and Mortality Worldwide for 36 Cancers in 185 Countries. CA. Cancer J. Clin. *71*, 209–249. https://doi.org/10.3322/caac.21660.

2. Rustgi, A.K., and El-Serag, H.B. (2014). Esophageal carcinoma. N. Engl. J. Med. *371*, 2499–2509. https://doi.org/10.1056/NEJMra1314530.

3. Pennathur, A., Gibson, M.K., Jobe, B.A., and Luketich, J.D. (2013). Oesophageal carcinoma. Lancet *381*, 400–412. https://doi.org/10.1016/S0140-6736(12)60643-6.

4. Baba, Y., Yoshida, N., Kinoshita, K., Iwatsuki, M., Yamashita, Y.I., Chikamoto, A., Watanabe, M., and Baba, H. (2018). Clinical and Prognostic Features of Patients With Esophageal Cancer and Multiple Primary Cancers: A Retrospective Single-institution Study. Ann. Surg. *267*, 478–483. https://doi.org/10.1097/SLA.0000000000002118.

5. Board, P.A.T.E. (2002). Esophageal Cancer Treatment (Adult) (PDQ(R)): Patient Version. In PDQ Cancer Information Summaries.

6. Yamamoto, S., and Kato, K. (2022). JUPITER-06 establishes immune checkpoint inhibitors as essential first-line drugs for the treatment of advanced esophageal squamous cell carcinoma. Cancer Cell *40*, 238–240. https://doi.org/10.1016/j.ccell.2022.02.009.

7. Doki, Y., Ajani, J.A., Kato, K., Xu, J., Wyrwicz, L., Motoyama, S., Ogata, T., Kawakami, H., Hsu, C.H., Adenis, A., et al. (2022). Nivolumab Combination Therapy in Advanced Esophageal Squamous-Cell Carcinoma. N. Engl. J. Med. *386*, 449–462. https://doi.org/10.1056/NEJMoa2111380.

8. Wang, Z.X., Cui, C., Yao, J., Zhang, Y., Li, M., Feng, J., Yang, S., Fan, Y., Shi, J., Zhang, X., et al. (2022). Toripalimab plus chemotherapy in treatment-naive, advanced esophageal squamous cell carcinoma (JUPITER-06): A multi-center phase 3 trial. Cancer Cell *40*, 277–288.e3. https://doi.org/10.1016/j.ccell.2022.02.007.

9. Kudo, T., Hamamoto, Y., Kato, K., Ura, T., Kojima, T., Tsushima, T., Hironaka, S., Hara, H., Satoh, T., Iwasa, S., et al. (2017). Nivolumab treatment for oesophageal squamous-cell carcinoma: an open-label, multicentre, phase 2 trial. Lancet Oncol. *18*, 631–639. https://doi.org/10.1016/S1470-2045(17)30181-X.

10. Baba, Y., Nomoto, D., Okadome, K., Ishimoto, T., Iwatsuki, M., Miyamoto, Y., Yoshida, N., and Baba, H. (2020). Tumor immune microenvironment and immune checkpoint inhibitors in esophageal squamous cell carcinoma. Cancer Sci. *111*, 3132–3141. https://doi.org/10.1111/cas.14541.

11. Doi, T., Piha-Paul, S.A., Jalal, S.I., Saraf, S., Lunceford, J., Koshiji, M., and Bennouna, J. (2018). Safety and Antitumor Activity of the Anti-Programmed Death-1 Antibody Pembrolizumab in Patients With Advanced Esophageal Carcinoma. J. Clin. Oncol. *36*, 61–67. https://doi.org/10.1200/JCO.2017.74.9846.

12. Xu, J., Li, Y., Fan, Q., Shu, Y., Yang, L., Cui, T., Gu, K., Tao, M., Wang, X., Cui, C., et al. (2022). Clinical and biomarker analyses of sintilimab versus chemotherapy as second-line therapy for advanced or metastatic esophageal squamous cell carcinoma: a randomized, open-label phase 2 study (ORIENT-2). Nat. Commun. *13*, 857. https://doi.org/10.1038/s41467-022-28408-3.

13. Kato, K., Cho, B.C., Takahashi, M., Okada, M., Lin, C.Y., Chin, K., Kadowaki, S., Ahn, M.J., Hamamoto, Y., Doki, Y., et al. (2019). Nivolumab versus chemotherapy in patients with advanced oesophageal squamous cell carcinoma refractory or intolerant to previous chemotherapy (ATTRACTION-3): a multicentre, randomised, open-label, phase 3 trial. Lancet Oncol. *20*, 1506–1517. https://doi.org/10.1016/S1470-2045(19)30626-6.

14. Huang, J., Xu, J., Chen, Y., Zhuang, W., Zhang, Y., Chen, Z., Chen, J., Zhang, H., Niu, Z., Fan, Q., et al. (2020). Camrelizumab versus investigator's choice of chemotherapy as second-line therapy for advanced or metastatic oesophageal squamous cell carcinoma (ESCORT): a multicentre, randomised, open-label, phase 3 study. Lancet Oncol. *21*, 832–842. https://doi.org/10.1016/S1470-2045(20)30110-8.

15. Kojima, T., Shah, M.A., Muro, K., Francois, E., Adenis, A., Hsu, C.H., Doi, T., Moriwaki, T., Kim, S.B., Lee, S.H., et al. (2020). Randomized Phase III KEYNOTE-181 Study of Pembrolizumab Versus Chemotherapy in Advanced Esophageal Cancer. J. Clin. Oncol. *38*, 4138–4148. https://doi.org/10.1200/JCO.20.01888.

16. Shen, L., Kato, K., Kim, S.B., Ajani, J.A., Zhao, K., He, Z., Yu, X., Shu, Y., Luo, Q., Wang, J., et al. (2022). Tislelizumab Versus Chemotherapy as Second-Line Treatment for Advanced or Metastatic Esophageal Squamous Cell Carcinoma (RATIONALE-302): A Randomized Phase III Study. J. Clin. Oncol. *40*, 3065–3076. https://doi.org/10.1200/JCO.21.01926.

17. Morad, G., Helmink, B.A., Sharma, P., and Wargo, J.A. (2021). Hallmarks of response, resistance, and toxicity to immune checkpoint blockade. Cell *184*, 5309–5337. https://doi.org/10.1016/j.cell.2021.09.020.

18. Balkwill, F.R., Capasso, M., and Hagemann, T. (2012). The tumor microenvironment at a glance. J. Cell Sci. *125*, 5591–5596. https://doi.org/10.1242/jcs.116392.

19. Quail, D.F., and Joyce, J.A. (2013). Microenvironmental regulation of tumor progression and metastasis. Nat. Med. *19*, 1423–1437. https://doi.org/10.1038/nm.3394.

20. Yao, J., Cui, Q., Fan, W., Ma, Y., Chen, Y., Liu, T., Zhang, X., Xi, Y., Wang, C., Peng, L., et al. (2020). Single-cell transcriptomic analysis in a mouse model deciphers cell transition states in the multistep development of esophageal cancer. Nat. Commun. *11*, 3715. https://doi.org/10.1038/s41467-020-17492-y.

21. Chen, Z., Zhao, M., Liang, J., Hu, Z., Huang, Y., Li, M., Pang, Y., Lu, T., Sui, Q., Zhan, C., et al. (2021). Dissecting the single-cell transcriptome network underlying esophagus non-malignant tissues and esophageal squamous cell carcinoma. EBioMedicine *69*, 103459. https://doi.org/10.1016/j.ebiom.2021.103459.

22. Zhang, X., Peng, L., Luo, Y., Zhang, S., Pu, Y., Chen, Y., Guo, W., Yao, J., Shao, M., Fan, W., et al. (2021). Dissecting esophageal squamous-cell carcinoma ecosystem by single-cell transcriptomic analysis. Nat. Commun. *12*, 5291. https://doi.org/10.1038/s41467-021-25539-x.

23. Dinh, H.Q., Pan, F., Wang, G., Huang, Q.F., Olingy, C.E., Wu, Z.Y., Wang, S.H., Xu, X., Xu, X.E., He, J.Z., et al. (2021). Integrated single-cell transcriptome analysis reveals heterogeneity of esophageal squamous cell carcinoma microenvironment. Nat. Commun.

12, 7335. https://doi.org/10.1038/s41467-021-27599-5.

24. Amin, M.B., Greene, F.L., Edge, S.B., Compton, C.C., Gershenwald, J.E., Brookland, R.K., Meyer, L., Gress, D.M., Byrd, D.R., and Winchester, D.P. (2017). The Eighth Edition AJCC Cancer Staging Manual: Continuing to build a bridge from a population-based to a more "personalized" approach to cancer staging. CA. Cancer J. Clin. *67*, 93–99. https://doi.org/10.3322/caac.21388.

25. Gay, C.M., Stewart, C.A., Park, E.M., Diao, L., Groves, S.M., Heeke, S., Nabet, B.Y., Fujimoto, J., Solis, L.M., Lu, W., et al. (2021). Patterns of transcription factor programs and immune pathway activation define four major subtypes of SCLC with distinct therapeutic vulnerabilities. Cancer Cell *39*, 346–360.e7. https://doi.org/10.1016/j.ccell.2020.12.014.

26. Joanito, I., Wirapati, P., Zhao, N., Nawaz, Z., Yeo, G., Lee, F., Eng, C.L.P., Macalinao, D.C., Kahraman, M., Srinivasan, H., et al. (2022). Single-cell and bulk transcriptome sequencing identifies two epithelial tumor cell states and refines the consensus molecular classification of colorectal cancer. Nat. Genet. *54*, 963–975. https://doi.org/10.1038/s41588-022-01100-4.

27. Sun, H., Wang, X., Wang, X., Xu, M., and Sheng, W. (2022). The role of cancer-associated fibroblasts in tumorigenesis of gastric cancer. Cell Death Dis. *13*, 874. https://doi.org/10.1038/s41419-022-05320-8.

28. Gunaydin, G. (2021). CAFs Interacting With TAMs in Tumor Microenvironment to Enhance Tumorigenesis and Immune Evasion. Front. Oncol. *11*, 668349. https://doi.org/10.3389/fonc.2021.668349.

29. Korsunsky, I., Millard, N., Fan, J., Slowikowski, K., Zhang, F., Wei, K., Baglaenko, Y., Brenner, M., Loh, P.R., and Raychaudhuri, S. (2019). Fast, sensitive and accurate integration of single-cell data with Harmony. Nat. Methods *16*, 1289–1296. https://doi.org/10.1038/s41592-019-0619-0.

30. Roychoudhuri, R., Eil, R.L., and Restifo, N.P. (2015). The interplay of effector and regulatory T cells in cancer. Curr. Opin. Immunol. *33*, 101–111. https://doi.org/10.1016/j.coi.2015.02.003.

31. Pagès, F., Berger, A., Camus, M., Sanchez-Cabo, F., Costes, A., Molidor, R., Mlecnik, B., Kirilovsky, A., Nilsson, M., Damotte, D., et al. (2005). Effector memory T cells, early metastasis, and survival in colorectal cancer. N. Engl. J. Med. *353*, 2654–2666. https://doi.org/10.1056/NEJMoa051424.

32. Kaech, S.M., Wherry, E.J., and Ahmed, R. (2002). Effector and memory T-cell differentiation: implications for vaccine development. Nat. Rev. Immunol. *2*, 251–262. https://doi.org/10.1038/nri778.

33. Martin, M.D., and Badovinac, V.P. (2018). Defining Memory CD8 T Cell. Front. Immunol. *9*, 2692. https://doi.org/10.3389/fimmu.2018.02692.

34. Jin, S., Guerrero-Juarez, C.F., Zhang, L., Chang, I., Ramos, R., Kuan, C.H., Myung, P., Plikus, M.V., and Nie, Q. (2021). Inference and analysis of cell-cell communication using CellChat. Nat. Commun. *12*, 1088. https://doi.org/10.1038/s41467-021-21246-9.

35. Liu, Z., Zhao, Y., Kong, P., Liu, Y., Huang, J., Xu, E., Wei, W., Li, G., Cheng, X., Xue, L., et al. (2023). Integrated multi-omics profiling yields a clinically relevant molecular classification for esophageal squamous cell carcinoma. Cancer Cell *41*, 181–195.e9. https://doi.org/10.1016/j.ccell.2022.12.004.

36. Sun, D., Guan, X., Moran, A.E., Wu, L.Y., Qian, D.Z., Schedin, P., Dai, M.S., Danilov, A.V., Alumkal, J.J., Adey, A.C., et al. (2022). Identifying phenotype-associated subpopulations by integrating bulk and single-cell sequencing data. Nat. Biotechnol. *40*, 527–538. https://doi.org/10.1038/s41587-021-01091-3.

37. Lu, Y., Wang, W., and Wang, F. (2023). Clinical benefits of PD-1 inhibitors in specific subgroups of patients with advanced esophageal squamous cell carcinoma: a systematic review and meta-analysis of phase 3 randomized clinical trials. Front. Immunol. *14*, 1171671. https://doi.org/10.3389/fimmu.2023.1171671.

38. Song, Y., Zhang, B., Xin, D., Kou, X., Tan, Z., Zhang, S., Sun, M., Zhou, J., Fan, M., Zhang, M., et al. (2023). First-line serplulimab or placebo plus chemotherapy in PD-L1-positive esophageal squamous cell carcinoma: a randomized, double-blind phase 3 trial. Nat. Med. *29*, 473–482. https://doi.org/10.1038/s41591-022-02179-2.

39. Wherry, E.J., and Kurachi, M. (2015). Molecular and cellular insights into T cell exhaustion. Nat. Rev. Immunol. *15*, 486–499. https://doi.org/10.1038/nri3862.

40. Chen, Q.Y., Li, Y.N., Wang, X.Y., Zhang, X., Hu, Y., Li, L., Suo, D.Q., Ni, K., Li, Z., Zhan, J.R., et al. (2020). Tumor Fibroblast-Derived FGF2 Regulates Expression of SPRY1 in Esophageal Tumor-Infiltrating T Cells and Plays a Role in T-cell Exhaustion. Cancer Res. *80*, 5583–5596. https://doi.org/10.1158/0008-5472.CAN-20-1542.

41. Smith, L.K., Boukhaled, G.M., Condotta, S.A., Mazouz, S., Guthmiller, J.J., Vijay, R., Butler, N.S., Bruneau, J., Shoukry, N.H., Krawczyk, C.M., and Richer, M.J. (2018). Interleukin-10 Directly Inhibits CD8(+) T Cell Function by Enhancing N-Glycan Branching to Decrease Antigen Sensitivity. Immunity *48*, 299–312.e5. https://doi.org/10.1016/j.immuni.2018.01.006.

42. Chen, J., Cao, Y., Markelc, B., Kaeppler, J., Vermeer, J.A., and Muschel, R.J. (2019). Type I IFN protects cancer cells from CD8+ T cell-mediated cytotoxicity after radiation. J. Clin. Invest. *129*, 4224–4238. https://doi.org/10.1172/JCI127458.

43. Borden, E.C. (2019). Interferons alpha and beta in cancer: therapeutic opportunities from new insights. Nat. Rev. Drug Discov. *18*, 219–234. https://doi.org/10.1038/s41573-018-0011-2.

44. Benci, J.L., Xu, B., Qiu, Y., Wu, T.J., Dada, H., Twyman-Saint Victor, C., Cucolo, L., Lee, D.S.M., Pauken, K.E., Huang, A.C., et al. (2016). Tumor Interferon Signaling Regulates a Multigenic Resistance Program to Immune Checkpoint Blockade. Cell *167*, 1540–1554.e12. https://doi.org/10.1016/j.cell.2016.11.022.

45. Koliński, T., Marek-Trzonkowska, N., Trzonkowski, P., and Siebert, J. (2016). Heat shock proteins (HSPs) in the homeostasis of regulatory T cells (Tregs). Cent. Eur. J. Immunol. *41*, 317–323. https://doi.org/10.5114/ceji.2016.63133.

46. van Eden, W., Jansen, M.A.A., Ludwig, I., van Kooten, P., van der Zee, R., and Broere, F. (2017). The Enigma of Heat Shock Proteins in Immune Tolerance. Front. Immunol. *8*, 1599. https://doi.org/10.3389/fimmu.2017.01599.

47. van Eden, W., van der Zee, R., and Prakken, B. (2005). Heat-shock proteins induce T-cell regulation of chronic inflammation. Nat. Rev. Immunol. *5*, 318–330. https://doi.org/10.1038/nri1593.

48. Li, M.O., and Rudensky, A.Y. (2016). T cell receptor signalling in the control of regulatory T cell differentiation and function. Nat. Rev. Immunol. *16*, 220–233. https://doi.org/10.1038/nri.2016.26.

49. Toker, A., and Ohashi, P.S. (2019). Expression of costimulatory and inhibitory receptors in FoxP3(+) regulatory T cells within the tumor microenvironment: Implications for combination immunotherapy approaches. Adv. Cancer Res. *144*, 193–261. https://doi.org/10.1016/bs.acr.2019.05.001.

50. Ko, K.P., Huang, Y., Zhang, S., Zou, G., Kim, B., Zhang, J., Jun, S., Martin, C., Dunbar, K.J., Efe, G., et al. (2023). Key Genetic Determinants Driving Esophageal Squamous Cell Carcinoma Initiation and Immune Evasion. Gastroenterology *165*, 613–628.e20. https://doi.org/10.1053/j.gastro.2023.05.030.

51. Deng, T., Wang, H., Yang, C., Zuo, M., Ji, Z., Bai, M., Ning, T., Liu, R., Wang, J., Ge, S., et al. (2022). Single cell sequencing revealed the mechanism of PD-1 resistance affected by the expression profile of peripheral blood immune cells in ESCC. Front. Immunol. *13*, 1004345. https://doi.org/10.3389/fimmu.2022.1004345.

52. Torre, D., Lachmann, A., and Ma'ayan, A. (2018). BioJupies: Automated Generation of Interactive Notebooks for RNA-Seq Data Analysis in the Cloud. Cell Syst. *7*, 556–561.e3. https://doi.org/10.1016/j.cels.2018.10.007.

STAR★METHODS

KEY RESOURCES TABLE

REAGENT or RESOURCE	SOURCE	IDENTIFIER
Deposited data		
ESCC patients scRNA-seq datasets	Zhang et al.,[22] Dinh et al.[23]	NCBI BioProject: PRJNA672851 PRJNA777911
PBMC scRNA-seq dataset (ICB tested patients)	Deng et al.[51]	Deng et al.[51]
Bulk RNA-seq dataset (ICB tested patients)	Liu et al.[35]	Genome Sequence Archive (GSA): HRA003107
Software and algorithms		
R and Python scripts	https://github.com/jaeilparklab/ESCC_project_2	RRID:SCR_002630
R 4.3.0	R Core Team, https://r-project.org/	RRID:SCR_001905
Python 3.8	Python Software Foundation, https://www.python.org/	RRID:SCR_008394
Scanpy	https://github.com/theislab/scanpy	RRID:SCR_018139
fGSEA	https://bioconductor.org/packages/fgsea	RRID:SCR_020938
pySankey2	https://github.com/SZJShuffle/pySankey2	N/A
CellChat	https://github.com/sqjin/CellChat	RRID:SCR_021946
Enrichr	http://amp.pharm.mssm.edu/Enrichr	RRID:SCR_001575
Scissor	https://github.com/sunduanchen/Scissor	RRID:SCR_002630
decoupleR	https://www.bioconductor.org/packages/release/bioc/html/decoupleR.html	RRID:SCR_006442
Graphpad Prism10	GraphPad Software https://www.graphpad.com/	RRID:SCR_002798

RESOURCE AVAILABILITY

Lead contact

Additional information and requests for resources and reagents should be directed to and will be fulfilled by the Lead Contact, Jae-Il Park (jaeil@mdanderson.org).

Materials availability

The materials will be available upon request.

Data and code availability

- scRNA-seq data are publicly available via the National Center for Biotechnology Information Sequence Read Archive (SRA) under the accession numbers PRJNA777911 and PRJNA672851.
- The code used to reproduce the analyses described in this manuscript can be accessed via GitHub (https://github.com/jaeilparklab/ESCC_project_2) and is publicly available as of the date of publication.
- Any additional information required to reanalyze the data reported in this paper is available from the lead contact upon request.

METHOD DETAILS

scRNA-seq data preparation

Public datasets

The raw read files of ESCC patient datasets were downloaded using the parallel-fastq-dump package and converted to fastq files. The fastq files were mapped to the GRCh38 reference genome using CellRanger (v7.0.1) pipeline. The datasets from 11 patients (NCBI

BioProject: PRJNA777911) were directly processed using the CellRanger, while 58 patients' datasets (NCBI BioProject: PRJNA672851) were separately input to CellRanger as CD45$^+$ and CD45- datasets were sorted during sample preparation. Single-cell dataset and patient information are described in Table S1.

scRNA-seq data analysis

Integration and clustering

The datasets from nine patients were preprocessed independently, and the CD45$^+$ cell clusters were retained for the immune cell population. 60 patients' dataset analysis was started with CD45$^+$ sorted datasets. After preprocessing procedures, 11 patients and 58 patients datasets were integrated using the "concatenate" function in Scanpy. A batch correction was conducted using "Harmony" implemented in Scanpy.[29] "Leiden" algorithm was used for clustering cells. Each cell cluster was annotated primarily with "B cell", "Fibroblast", "Mast cell", "Myeloid cell", and "T cell" using marker genes of each cluster. T cells were further annotated with "CD4 T cell", "CD8 T cell", "exhausted T cell", and "effector T cell". Myeloid cells were further annotated into "Monocyte", "Macrophage", "M1 Macrophage", and "M2 Macrophage" clusters.

Classification of each cell type

"T cell", "Myeloid cell", "B cell", "Fibroblast", "Mast cell", "Plasma cell", and "Mixed" clusters were isolated, and each cell type was analyzed with individual patients. The transcriptomic similarity of each patient was compared using the correlation matrix function in Scanpy. Dendrograms were drawn to show PCA proximity, and Pearson correlation was displayed with color code. Patients were clustered and classified based on the result of the correlation matrix. Patients were classified by the T cell, myeloid cell, and fibroblast transcriptomes-based categories, then connected classifications such as Myeloid cell-T cell (MT) and B cell-T cell (BT) were applied to each patient. The connected classification of each patient was visualized with a Sankey plot using the "pysankey2" package.

Cell-to-cell interaction analysis

The "CellChat" package was used for cell-to-cell interaction inference. To acquire intercellular interactions, tumor cell datasets were added to immune cell datasets. For 11 patient datasets, excluded CD45-cell clusters were re-integrated into the immune cell datasets. For 58 patients' datasets, CD45$^+$ datasets were analyzed from separated matrix files. After preprocessing tumor cells, "Tumor cells", "effector T cell", "exhausted T cell", "CD4 T cell", "CD8 T cell", "M1 macrophage", "M2 macrophage", "Macrophage", "Monocyte", "B cell", "Fibroblast", and "Mast cell" clusters were merged. MT or FT classification-based patient groups were used to generate gene expression matrices for the CellChat analysis. From significant signaling pathways, "IL1", "IL16", "IL10", and "IFN-II" signaling were specified for analysis in each group of patients. Comparative analysis was performed using two different groups of patients (m1t4 vs. m2t3 and m3t4 vs. m2t3).

fGSEA analysis

"fGSEA" package was used for the GSEA analysis of m1t4, m2t3, m3t4, F1t4, and F4t3 groups of patients. "Epithelial cells", "Myeloid cell", "T cell", and "Fibroblast" clusters were independently analyzed to obtain a differentially expressed gene (DEG) list. DEG was performed in Scanpy with the "rank_gene_groups" function using the "Wilcoxon" method. The "C2" category and "REACTOME" subcategory or "C5" category and "GO:BP" subcategory were used to use each database. GSEA results are listed in Tables S2, S3, and S4.

Principal components analysis (PCA)

Transcriptomic proximity was evaluated by PCA analysis and visualized using a dendrogram. For comparison of MT groups and PBMCs, TME cells of MT groups and all PBMC cells were integrated and batch-corrected using 'Scanpy' and 'Harmony' packages. To compare transcriptomes of MT groups and Tumor-R and -NR bulk RNA-seq, the single-cell information of datasets of MT groups (tumor cells and TME cells) were reduced into grouped information using a "decoupler" package. This pseudo bulk RNA-seq information generated from MT groups was integrated with Tumor-R and Tumor-NR gene expression raw count matrix. The integrated gene expression matrix was normalized together, and PCA analysis was performed using the "Scanpy" package.

PBMCs scRNA-seq data analysis

Integration and clustering

PBMCs scRNA-seq datasets from anti-PD-1 therapy were provided by Dr. Haiyang Zhang.[51] Patients were classified into partial response (PR, defined as a ≥30% reduction in the sum of maximum diameters of lesions for at least 4 weeks), stable disease (SD, characterized by lesions with no reduction or enlargement), or progressive disease (PD, indicated by a ≥20% increase in lesion diameter or the appearance of new lesions). The PR or SD patients were collectively identified as the immunotherapy-sensitive group, referred to as PBMC-R in this study, while PD cases comprised the immunotherapy-resistant group, annotated as PBMC-NR. Three PBMC-R and three PBMC-NR gene expression matrix files were independently preprocessed and integrated. The batch effect was reduced by Harmony algorithm,[29] and cell types were annotated with markers used in the previous study.[51] PBMC datasets were further integrated with 69 patients' human ESCC datasets with the same workflow and analyzed.

fGSEA analysis

As described above, fGSEA analyses were performed with isolated T cells with DEG lists between responders and non-responders. REACTOME database was used, and the results were compared with human ESCC patient fGSEA results. GSEA results of PBMCs are listed in Table S5.

Pathway score analysis

The Pathway scores were performed using the "scanpy.tl.score_genes" function implemented in the Scanpy package. The analysis was done with default parameters and the reference genes from MSigDB and other literature. Reference genes were listed in Table S6.

Bulk RNA-seq data analysis
Data preprocess

The raw count datasets of anti-PD-1 treated patients were provided by Dr. Liu.[35] For classification for therapeutic responses, patients were categorized as PR, PD, and SD after intravenous administration of anti-PD-1 (SHR-1210) at doses ranging from 60 mg to 400 mg, with 4-week interval after the first dose followed by a 2-week schedule. Leveraging multi-omics profiling, IM and non-IM groups were delineated, which were annotated in this study as Tumor-R and Tumor-NR, respectively. The raw counts were grouped into Tumor-R and Tumor-NR to calculate differentially expressed genes (DEG). DEG matrix was generated using the "DESeq2" R package. The raw counts were converted to log2 FPKM for further analysis using "DGEobj.utils" R package.

fgsea and enrichr analysis

"fGSEA" package-based analysis between Tumor-R and Tumor-NR was conducted using the DEG list as described above. Rank genes were generated from the filtered DEG list with *P* value (<0.05) criteria, and "REACTOME" and "GOBP" subcategories of databases were used. Shared signaling pathways with other groups were visualized using Venn diagrams with the "ggvenn" R package. The Enrichr analysis was conducted using raw counts in the BioJupies analytic tools.[52]

Scissor analysis

The "Scissor" R package was used for transcriptomic comparison between bulk RNA-seq (Tumor-R and -NR) and scRNA-seq (m1t4, m2t3, and m3t4). Gene expressions of bulk RNA-seq were binarized by ICI response (Tumor-R and -NR). Tumor cells and TME cells of m1t4, m2t3, and m3t4 groups were integrated independently in "Scanpy", and the datasets were converted to Seurat object with raw counts and cluster information. Each group was normalized and preprocessed in Seurat. Scissor analyses were performed with binarized gene expression information and single cells of each group using the same parameter (alpha = 0.01). Scissor+ and Scissor- cells represented ICI-responder-like cells (Tumor-R+) and -Non-responders-like cells (Tumor-NR+).

QUANTIFICATION AND STATISTICAL ANALYSIS

The Student's *t*-test was used to compare two groups (n ≥ 3), and a one-way analysis of statistical variance evaluation was used to compare at least three groups (n ≥ 3). *P* values < 0.05 were considered significant. Error bars indicate the standard deviation (s.d.). All experiments were performed three or more times independently under identical or similar conditions.